RSC Advances

ROYAL SOCIETY OF CHEMISTRY

www.rsc.org/advances

TOC

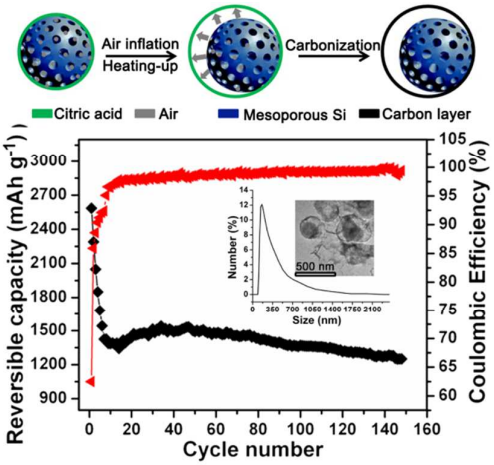

A novel method was developed to prepare mesoporous Si/C nanocomposites with yolk-shell structure (MSi@C) successfully. The obtained nanocomposites showed good retention of specific capacity (1264.7 mAh g^{-1} even after 150 cycles with high coulombic efficiency above 99%). This work provides an alternative method to fabricate yolk-shell structured materials.

Cite this: DOI: 10.1039/c0xx00000x

www.rsc.org/xxxxxx

ARTICLE TYPE

A novel approach to prepare Si/C nanocomposites with yolk-shell structure for lithium ion batteries

Huan-Huan Li,[a] Jia-Wei Wang,[b] Xing-Long Wu,[a] Hai-Zhu Sun,*[a] Feng-Mei Yang,[a] Kang Wang,[a] Lin-Lin Zhang,[a] Chao-Ying Fan,[a] Jing-Ping Zhang*[a]

Received (in XXX, XXX) Xth XXXXXXXXX 20XX, Accepted Xth XXXXXXXXX 20XX
DOI: 10.1039/b000000x

A novel method was developed to successfully prepare mesoporous Si/C nanocomposites with yolk-shell structure (MSi@C). Different from the reported methods, this approach was unique, straightforward and easily scaled up. A plausible mechanism for the formation of MSi@C nanocomposites was proposed, which was in accordance with the results of transmission electron microscope (TEM). When the mixture of mesoporous Si (M-Si) and citric acid was heated up, the volume of air adsorbed by the M-Si expanded, and the viscoelastic citric acid layers inflated just like balloons, directly leading to the formation of the yolk-shell structured MSi@C nanocomposites during the carbonization. The MSi@C nanocomposites possessed an M-Si core with diameter ~150 nm and a carbon shell with diameter ~230 nm. Such nano and mesoporous structure combined with voids between M-Si core and carbon shell, not only provides enough space for the volume expansion of M-Si during lithiation, but also accommodates the mechanical stresses/strains caused by the volume inflating and contraction. Moreover, partially graphitization of the carbon contributed to the improved electrical conductivity and rate performance of MSi@C. As a result, the prepared MSi@C exhibited an initial reversible capacity of 2599.1 mAh g^{-1} and maintained 1264.7 mAh g^{-1} even after 150 cycles at 100 mA g^{-1}, with high coulombic efficiency (CE) above 99% (based on the weight of M-Si in the electrode). Therefore, this work provided an alternative method to fabricate yolk-shell nanostructured materials with great potential as anode materials for lithium ion batteries.

Introduction

Recently, lithium ion batteries have attracted much attention due to the rapid development of portable electronic devices, electric vehicles (EVs), and hybrid electric vehicles (HEVs).[1-6] This naturally drives the intense research interests towards new electrode materials with higher energy density and longer cycle life. Among various anode materials, Si is one of the most promising anodes because of its highest theoretical specific capacity (4200 mAh g^{-1}),[7-9] abundance in the earth crust and low lithiation potential,[10] etc. Unfortunately, Si anode materials exhibit poor cycling property resulted from its huge volume change (>300%) during the charge/discharge processes.[7, 11-15]

Many investigations based on Si anodes focus on overcoming the huge morphological change and improving the electric conductivity. One way to relieve the problem is to reduce the size of Si particles to nanoscale.[16, 17] Not only are nanostructured Si based anodes more resistant to the variance of volume, but also the small size shortens the diffusion path of lithium ions. It has been shown that nanostructured Si based anodes such as nanoparticles,[18] nanowires,[12, 19-22] nanospheres[23, 24] and nanotubes,[25] etc. present obvious improvement in their cycle lifetime. However, pure Si nanoparticles are easily aggregated especially during lithiation/delithiation processes, resulting in invalidation of electronic transport pathways during cycling.[26] Incorporating the nanostructured Si into an electrochemically inactive matrix is an effective strategy to overcome this problem.[13, 27-30] The inactive phase can stabilize Si nanomaterials, prevent the aggregation of nanoparticles and accommodate the mechanical stresses/strains caused by volume change of Si and enhance their conductivity.

Since a novel yolk-shell structured Au@polymer have been synthesized and characterized by Xia and *co*-workers,[31] this special structure has drawn tremendous interests because of their unique physical-chemical characteristics, such as low density, high specific area, and the large void volume.[32-35] Especially, unlike normally core-shell structured anodes, the void space between the yolk and shell allows for the active materials to expand upon lithiation without breaking the shell, thus ensuring the stability of the solid electrolyte interface (SEI) layer.[36] So encapsulating Si nanoparticles into elastic hollow carbon spheres becomes another ideal strategy to alleviate the volume change and aggregation problems.

So far, many electrode materials with yolk-shell structure have been successfully prepared and showed good electrochemical performance.[34, 35, 37-41] To the best of our knowledge, almost all of them were obtained by etching SiO_2@C to form voids using NaOH or HF aqueous solution.[35, 42, 43] Although selective etching method is very useful in fabricating yolk-shell structured materials with desirable nanostructures, compositions and sizes,

the method has some intrinsic drawbacks as it generally involves multiple tedious steps, making large scale production difficult.[44] Therefore, the aim of this study is to develop a straightforward approach to prepare yolk-shell structured materials with decent electrochemical properties. Encouragingly, a mesoporous Si and carbon nanocomposite with yolk-shell structure (MSi@C) was successfully prepared by a new method, and the process of forming yolk-shell structure was unique and straightforward. The obtained MSi@C nanocomposites exhibited an initial reversible capacity of 2599.1 mAh g^{-1} and maintained 1264.7 mAh g^{-1} even after 150 cycles at 100 mA g^{-1}, with high coulombic efficiency (CE) above 99% (based on the weight of M-Si in the electrode). Moreover, the MSi@C nanocomposites presented good rate performance that the first reversible capacities of 2128.3, 1803.5, 849.2 mAh g^{-1} at the current densities of 300, 500 and 1000 mA g^{-1} had been reached, respectively.

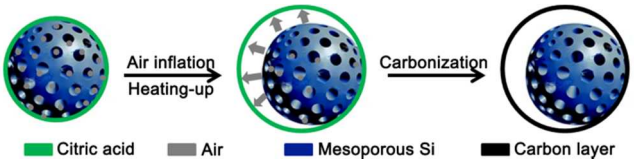

Scheme 1. The formation process of MSi@C nanocomposites with yolk-shell structure (grey arrows represent the expansion direction of air).

Experimental section

Solvents and starting materials were purchased from Aladdin and used as received without further purification unless noted. Firstly, 0.846 g cetyltrimethyl ammonium bromide (CTAB) and 0.082 g polyoxyethylene (10) cetyl ether (Brij-56) were dissolved in buffer solution (250 mL) to form a homogeneous solution by ultrasonication for 1 h. Then 4.2 mL of tetraethoxysilane (TEOS) was added drop by drop when the buffer solution was heated to 95°C. After vigorous stirring for 8 h at 95°C, the resulting products were purified by centrifugation with ethanol, distilled water and then dried at 80°C overnight. After that, the synthesized inorganic-organic composite was calcined at 550°C for 3 h to remove the organic surfactants. When the surfactants were totally decomposed under air atmosphere, the porosity was obtained.

Secondly, one mole of mesoporous SiO_2 together with two moles of Mg was ground in the porcelain boat to form a uniform dark gray mixture.[8, 45] Then the boat was sealed with a stainless-steel chamber and heated at 650°C for 6 h under the flowing gas (5 vol% hydrogen and 95 vol% argon). The obtained Mg/MgO/Si black mixture was first immersed by 1 mol L^{-1} HCl solution for 2 h to remove MgO. The resulting mesoporous silicon was washed with absolute alcohol and distilled water for several times and then vacuum-dried at 80°C overnight. Thirdly, citric acid (CA) and mesoporous Si (M-Si) were mixed with the molar ratio of 1:1 in anhydrous alcohol to form a uniform solution by ultrasonication. When ethanol was almost completely evaporated, the sticky mixture was calcined at 700°C (3°C min^{-1}) for 4 h under N_2 atmosphere to get MSi@C nanocomposites. The spray-pyrolysis reaction of Si and CA can be expressed as Equation (1) .[29]

$$Si + C_6H_8O_7 \rightarrow Si/C + CO_2 \uparrow + H_2O \uparrow + \text{energy} \uparrow \quad (1)$$

Scheme 1 illustrates the formation process of yolk-shell structured MSi@C nanoparticles. The structure of the obtained M-Si and MSi@C was characterized by X-ray diffraction (XRD, Rigaku P/max 2200VPC) using Cu Kα radiation. The carbon content was determined by thermogravimetric analysis (TGA) with a heating rate of 10°C min^{-1} carried out in air. To confirm the existence of mesopores on the surface of Si, nitrogen adsorption isotherms at −196°C for mesoporous Si was adopted. Transmission electron microscope (TEM, JEM-2010F) was used to further study the morphology of the products. Particle size and distribution were tested by Zetasizer NanoZS (Malvern Instruments). Raman measurement was performed with a JY HR-800 Lab Ram confocal Raman microscope in a backscattering configuration with an excitation wavelength of 514.4 nm. The electrochemical impedance spectroscopy (EIS) measurements were carried out in two-electrode cells on Par 2273 Potentiostats-Electrochemistry Workstation with a ±5 mV ac signal amplitude and frequency ranged from 10 kHz to 0.1 Hz.

The anodes were prepared by mixing the active material powders (70 wt%), acetylene black (15 wt%), and polyvinylidene fluoride (PVDF) binder (15 wt%) in *N*-methyl-2-pyrrolidione (NMP) to produce a homogeneous slurry, then coating the slurry onto copper foils. Pure lithium foil was used as the counter electrode and a 1.0 M $LiPF_6$ in 1:1 v/v ethylene carbonate (EC)/dimethyl carbonate (DMC) as the electrolyte.

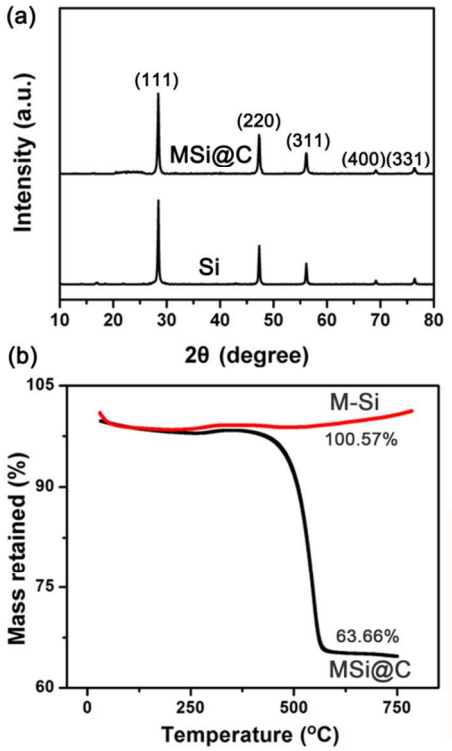

Fig. 1 (a) XRD patterns of MSi@C and M-Si nanoparticles. (b) TGA curve of M-Si and MSi@C nanocomposites measured under air atmosphere.

Cite this: DOI: 10.1039/c0xx00000x

www.rsc.org/xxxxxx

ARTICLE TYPE

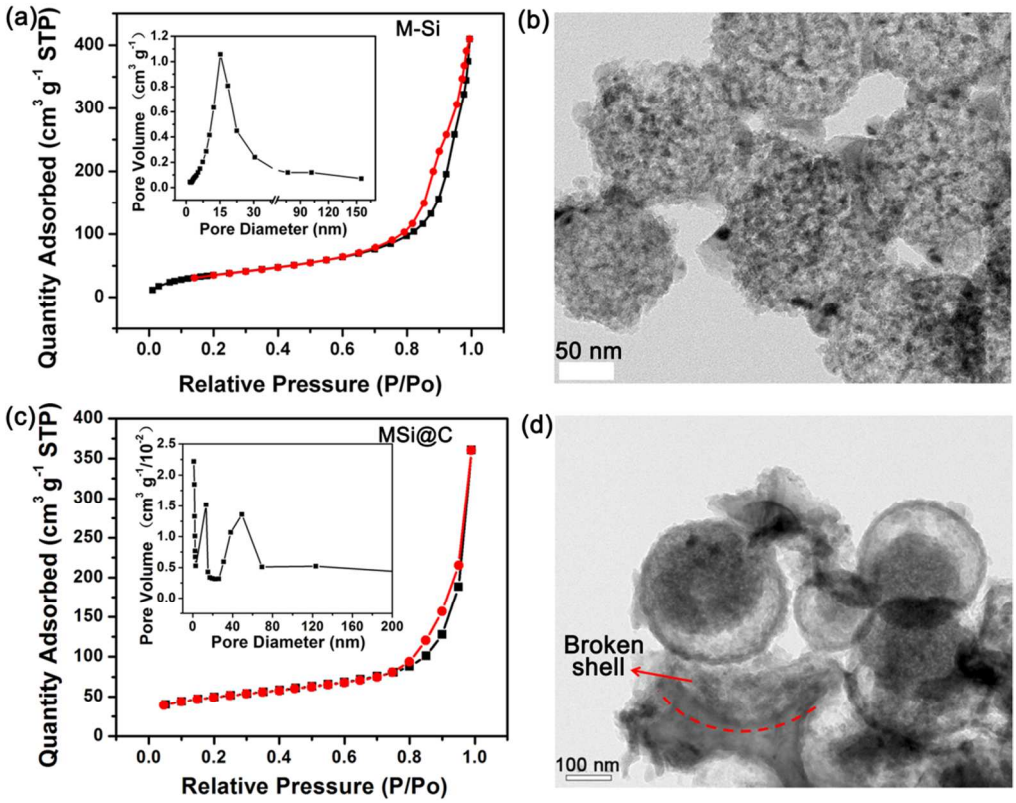

Fig. 2 Nitrogen adsorption isotherms at −196°C for (a) M-Si and (c) MSi@C, the insert shows the BJH pore size distribution. FE-TEM image of (b) M-Si nanoparticle and (d) MSi@C nanocomposites.

The 2025 coin cells were assembled in an Ar-filled glovebox. Galvanostatic cycling measurements were made using a Land battery test system from 0.01 to 1.5 V.

Results and discussion

XRD and TGA analysis

The XRD patterns of the prepared M-Si and MSi@C are shown in Fig. 1a. It's evident that the sharp peaks at 2θ of 28.4°, 47.4°, 56.2°, 68.2°, and 76.4° correspond to (111), (220), (311), (400) and (331) planes of crystal Si, respectively. The peak positions and shapes of MSi@C are almost identical with those of Si, which indicates that the crystal forms of Si are remained after heat treatment at 700°C under N_2 atmosphere. Moreover, the broad peak appears at around 2θ = 24°, implying the predominately amorphous nature of the carbon in MSi@C. The TGA curve of the MSi@C carried out under air atmosphere (Fig. 1b) shows that the Si content in the composite is ~64 wt%, and that of carbon is ~36 wt%. It's important to note that the silicon can be oxidized to silicon dioxide when heated in air or oxygen, but this oxidation reaction will not happen unless the temperature comes to above 800°C under the atmospheric pressure. The thermogravimetric analysis of pristine Si exhibits weight gain at 1070°C, and the silicon oxidation process is completed at temperatures above 1200°C.[46] In our system, because the TGA curve of the MSi@C nanocomposite was carried out from room temperature to 750°C (bellow 800°C) under air atmosphere, it can be seen that there almost no oxidation reaction could be found and the weight gain of M-Si is only 0.57% (Fig. 1b).

Morphologies and formation mechanism of MSi@C

To confirm the existence of mesopores on the surface of Si, nitrogen adsorption isotherms at −196°C for M-Si were performed. From Fig. 2a, the nitrogen adsorption isotherms of M-Si have the characteristic of materials with large mesopores (type IV).[47, 48] In addition, a very distinct hysteresis loop on its desorption isotherm (H-1) is another characteristic of mesopore materials. The pore size distribution (PSD) (inset Fig. 2a) was calculated by using Barrett−Joyner−Halenda (BJH) method, which was about 15 nm. As shown in Fig. 2b, the diameter of the M-Si is ~150 nm, with pores uniformly distributed on its surface. It has been reported that there existed a critical particle diameter of ~150 nm for Si. The particles with size larger than 150 nm would initially form surface cracks and then fracture due to lithiation-induced swelling while those with size smaller than 150 nm would neither presented crack nor fracture upon first lithiation.[49] As the size for most of the M-Si nanoparticles prepared in this work is smaller than 150 nm, the volume change

can be effectively alleviated. Moreover, the mesoporous structure is believed to provide required space for the volume expansion and hence is favourable for the cycle performance of materials. As a result, it can be expected that M-Si will possess a decent electrochemical properties.

As shown in Fig. 2c, the nitrogen adsorption isotherms at −196°C for MSi@C was also performed. It can be seen that the yolk-shell structured MSi@C nanocomposite not only shows pores centered at ~15 nm, but also exhibits another two new sized pores, which come from the carbon shell and voids between M-Si and carbon layer. FE-TEM image of the MSi@C nanocomposite clearly reveals the yolk-shell feature. The TEM image exhibits that the MSi@C nanocomposite with a shell thickness about 10 nm, and the diameters of the shell and core are ~230 and ~150 nm, respectively. A plausible explanation of forming yolk-shell structure is proposed in Scheme 1. Firstly, the citric acid in ethanol solution has high viscosity and elasticity, making it easy to closely coating on the surface of M-Si. When heated up, the air absorbed by M-Si expanded and the most citric acid layers inflated, just like balloons, directly leading to the formation of the yolk-shell structure during the carbonization. Some broken shells caused by over inflation of the adsorbed air could also be seen in Fig. 2c. In order to verify this proposed mechanism, the individual volume of spherical MSi@C nanocomposite at the carbonization temperature (T_c) of CA was calculated and compared with the result obtained from TEM. To simplify the calculation, the gas in the mesoporous of M-Si was considered as ideal gas and it was assumed that the change of volume was carried out under a constant pressure process. In addition, because the CA was deposited on the surface of M-Si, the CO_2 and H_2O decomposed from the CA during carbonization would fan out to outsides of M-Si, which was not considered in this calculation. According to the analysis above, the volume change during the carbonization may be estimated by the following equations:

Table 1 Equivalent circuit parameters of M-Si and MSi@C obtained from fitting the experimental impedance spectra.

Sample	R_e (Ω)	R_f (Ω)	R_{ct} (Ω)
M-Si	5.26	24.23	93.88
MSi@C	5.27	17.68	37.88

$$V_{void} = 4\pi / 3(R_{shell}^{3} - R_{yolk}^{3}) \quad (1)$$

$$V_{total\,pore} = m_{Si} \times V_{pore} = \rho_{Si} 4\pi / 3 R_{yolk}^{3} \times V_{pore} \quad (2)$$

$$V_{\exp and} = V_{void} + V_{total\ pore} \quad (3)$$

$$PV_{total\ pore} = nRT_{room},\ PV'_{\exp and} = nRT_{c} \quad (4)$$

Where R_{shell} (115 nm) and R_{yolk} (75 nm) are the semidiameters of the carbon shell and M-Si, respectively (Fig. 2d), ρ_{Si} is 2.33 g cm^{-3}, V_{pore} is 0.6371 cm^3 g^{-1} (obtained from result of the BET), and $V_{total\ pore}$ is the pore volume of individual M-Si nanoparticle. T_{room} is the room temperature (293.15K) and T_c is the actual carbonization temperature of CA (~ 773.15K, obtained from Fig. 1b). According to equations (1) to (4), the calculated V'_{expand} was ~6.9×10^{-15} cm^3, which was quite close to the V_{expand} (~7.2×10^{-15} cm^3) obtained from TEM and DLS, verifying the mechanism we proposed. It is expected that such nano-, mesoporous, and yolk-shell structure will endow the MSi@C composite with stable electrochemical properties.

Raman spectra and EIS analysis

The graphitization degree of the carbon is analyzed by Raman spectrum shown in Fig. 3a. Three characteristic peaks at about 500, 1350, and 1580 cm^{-1} are assigned to the typical mode of crystalline Si, D- and G-bands of carbon, respectively. The I_D/I_G ratio of the MSi@C nanocomposite was estimated to be 0.71, indicating the semi-amorphous nature of the carbon in the composite. As shown in Fig. 3b, EIS measurements were carried out to gain further insight into the electrochemical performance of MSi@C after the fifth discharge-charge cycle. Inset of Fig. 3b is the modified equivalent circuit used from which the key kinetic parameters are obtained by simulation. Table 1 shows the fitting impedance data, including the resistance for lithium ion (Li^+) transport in the electrolyte (R_e), Li^+ migration through the surface film (R_f) and charge transfer resistance between the electrolyte interface and electrode (R_{ct}) for both M-Si and MSi@C composite. Because the use of electrolyte is the same for M-Si and MSi@C electrodes, the R_e is close to each other. Seen in Table 1, The R_f

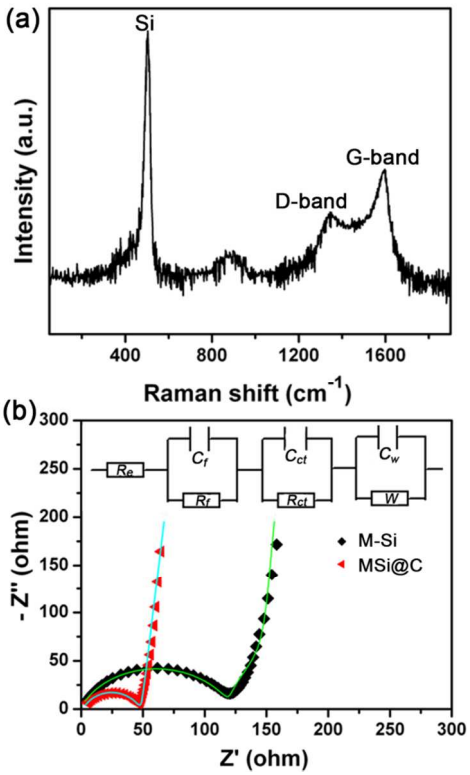

Fig. 3 (a) Raman spectra of MSi@C nanocomposites after annealing at 700ºC. (b) Nyquist plots of M-Si and MSi@C nanocomposite electrodes after the fifth discharge-charge cycle, inset is the equivalent circuit.

Cite this: DOI: 10.1039/c0xx00000x

www.rsc.org/xxxxxx

ARTICLE TYPE

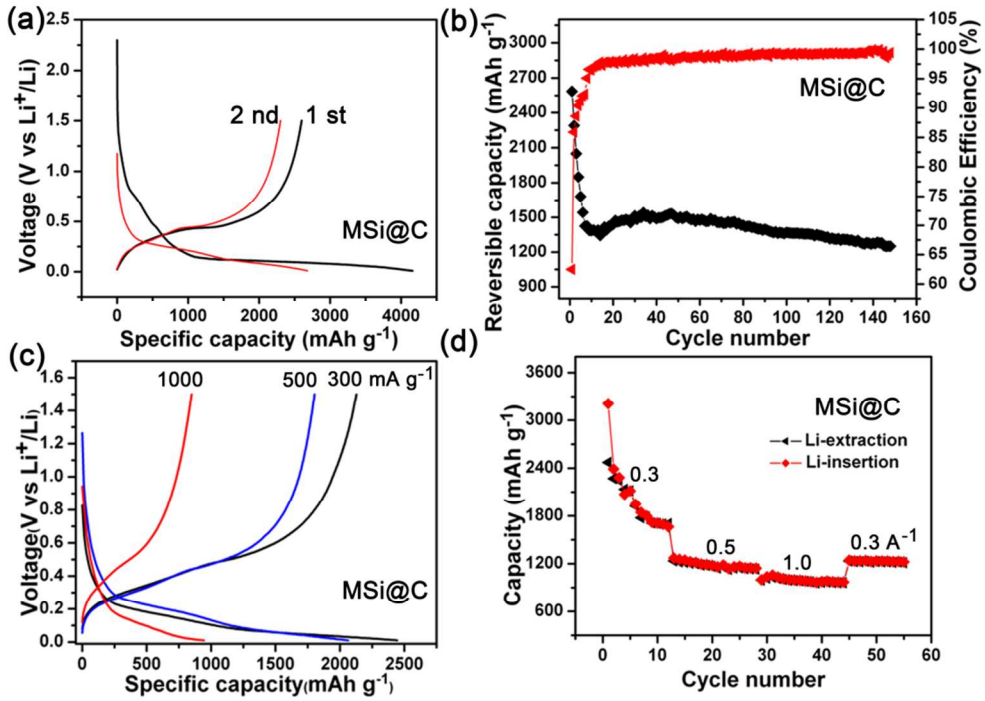

Fig. 4 (a) The first two-cycle charge-discharge profiles and (b) cycle performance of MSi@C electrode under 100 mA g^{-1}. (c) The second charge-discharge profiles of MSi@C electrode under different current densities. (d) Rate performance of MSi@C electrode

(17.68 Ω) of MSi@C is smaller than that (24.23 Ω) of M-Si, implying that the carbon shell makes the migration of Li^+ through the electrolyte more easily. Moreover, smaller Rct (37.98 Ω) of MSi@C indicates that the carbon layer contributes to maintaining the electronic contact during the cycles. It can be concluded from these results that better electrochemical properties will be obtained for MSi@C nanocomposite than M-Si.

Electrochemical performance of MSi@C

Fig. 4a shows the first two-cycle charge-discharge profiles of MSi@C electrode under current of 100 mA g^{-1}. The first reversible capacity of MSi@C electrode is 2599.1 mAh g^{-1}. Note that the initial CE is 62.8%, corresponding to an irreversible capacity (Q_{irr}) of 1540 mAh g^{-1} (37.2%). The low CE for the first cycle is mainly due to the formation of the SEI layer by the decomposition of electrolyte on the surface of MSi@C. It can be seen that the Q_{irr} of the second cycle is 240.6 mAh g^{-1}, which is much smaller than that of the first cycle. Moreover, the MSi@C presents good cycle performance that the reversible capacity is still as high as 1264.7 mAh g^{-1} even after 150 cycles (Fig. 4b), with the CE above 99%. As shown in Fig. 4c, the MSi@C electrode shows high reversible capacities of 2128.3, 1803.5, 849.2 mAh g^{-1} at the current densities of 300, 500 and 1000 mA g^{-1}, respectively. Especially, the MSi@C electrode maintains high stable reversible capacities with increasing current densities (Fig. 4d). The interesting results show that the capacity at 100 mA g^{-1} decays much faster than that of 300 mA g^{-1}. This is due to the

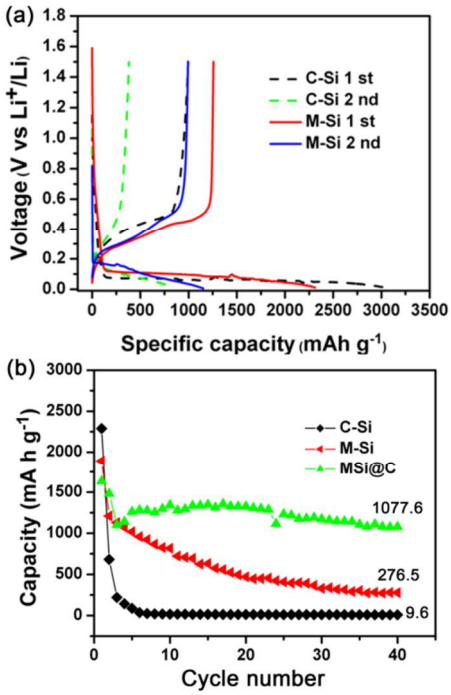

Fig. 5 (a) The first two charge-discharge profiles of C-Si and M-Si tested at 100 mA g^{-1}. (b) Cycle performance of C-Si, M-Si and MSi@C under 500 mA g^{-1}.

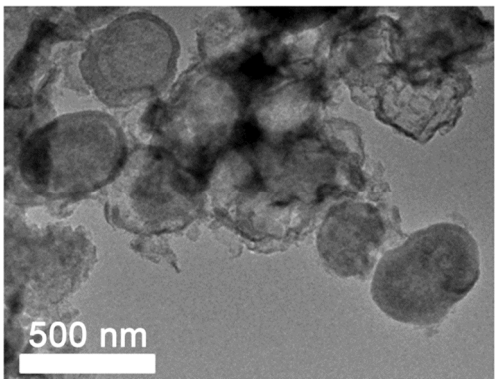

Fig. 6 FE-TEM image of MSi@C nanocomposites after 30 cycles under 100 mA g^{-1} with charged station.

following two reasons: 1) when charging at a relatively low current density, the full reduction of Si to 0.01 V induces that it is difficult to complete extraction of Li^+ ions at consequent charge process; 2) at a low current density, the charge and discharge depth is more extensive, which may bring about a collapse of the crystallographic structure of this material. This phenomenon is also found in other report.[50] The decent electrochemical performance of the MSi@C electrode can be attributed to the following reasons:

(a) Nano- and mesoporous structure

It is believed that the nano- and mesopores can effectively alleviate the problem brought by volume change. In order to verify the contribution of mesopores to the improved electrochemical performance, the charge-discharge tests of commercially available Si (C-Si, purchased from Alfa Aesar, APS=100 nm, 99.9%) were performed. As shown in Fig. 5a, though the C-Si shows high first discharge capacity, the Q_{irr} is as high as 1982.1 mAh g^{-1} (65.2%), and a rapid capacity loss is observed in the second cycle. As the C-Si nanoparticles neither completely belong to nanoscale nor have porous structure, there is no surprise that they show poor cycle performance, indicating the importance of mesoporous structure.

(b) Carbon shell in the yolk-shell structure

Carbon shells with partially crystallization are beneficial to both electron and ion transport, which lead to good kinetics, making it possible for electrons and Li^+ to fast transmit from current collector to active materials. In addition, the carbon shell is a self-supporting framework, the void spaces between M-Si and carbon shell provide effective room for the expansion of M-Si during lithiation processes. This can be confirmed by comparing the electrochemical properties of MSi@C with that of the M-Si, which were investigated in order to prove the function of the carbon shells. Fig. 5a also gives the charge-discharge profiles of M-Si electrode under rate of 100 mA g^{-1}. The existence of mesopores does alleviate the expansion of M-Si and the electronic contact maintains relatively better during the charge-discharge processes compared with C-Si. As a result, the first discharge and charge capacities of M-Si electrode were 2312.7 mAh g^{-1} and 1258.3 mAh g^{-1}. The Q_{irr} is 45.6%, which is much lower than that of C-Si, but still higher than that of MSi@C. Above all, the MSi@C exhibits better rate properties than M-Si and C-Si. Fig. 5b shows the capacity retention of C-Si, M-Si and MSi@C at the current density of 500 mA g^{-1}. It's clearly seen that after 40 cycles, the reversible capacity of MSi@C is 1077.6 mAh g^{-1}, which is much higher than those of C-Si (9.6 mAh g^{-1}) and M-Si (276.5 mAh g^{-1}). The MSi@C shows better rate properties because it possess lower R_f (17.68 Ω) and R_{ct} (37.98 Ω) (Table 1), which results from the carbon shell. As shown in Fig. 6, after 30 cycles, most of the carbon shells were not broken even the MSi@C was under fully Li^+ insertion station.

(c) Electrochemical stability of the MSi@C

Fig. 7 displays the CV curves of the MSi@C performed in EC/DMC containing 1 M $LiPF_6$ between 0.01 and 1.5 V at a scan rate of 0.5 mV s^{-1}. In the first scanning cycle, there are two cathodic peaks located at 1.2 and 0.7 V, which disappear from the second cycle. The peak at 1.2 V is attributed to the reduction of silicon oxide species,[51] and the irreversible cathodic peak at 0.7 V results from the reversible electrolyte reduction and the formation of a solid electrolyte interface (SEI) layer on the surface of the MSi@C electrode. On the reverse scan, two anodic peaks located at 0.36 and 0.56 V are attributed to the extraction of lithium ions from Li-Si alloys. The two anodic peaks gradually evolve from

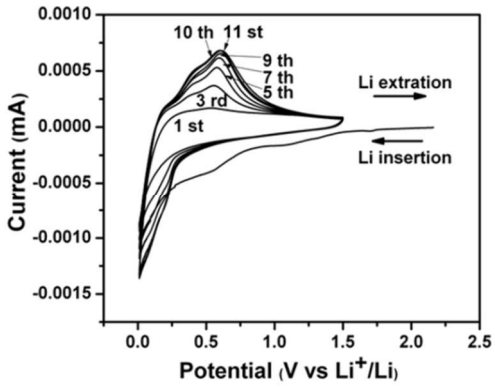

Fig. 7 Cyclic voltammetry of MSi@C nanocomposites from 0.01 to 1.5 V vs. Li/Li^+ at a scan rate of 0.5 mV s^{-1}.

first scanning cycle until 10^{th} cycle, and the 11^{st} curve is completely superimposed on the 10^{th}. This indicates that the electrode reaches an electrochemical stability after 10^{th} cycle. This result shows that the nano- and mesoporous, yolk-shell structure is much helpful to maintain the stability and integrity of the nanostructure.

Conclusions

In summary, we developed a novel method to synthesize materials with yolk-shell structure. Using this approach, yolk-shell structured MSi@C nanocomposite was successfully designed and fabricated. When evaluated as anode for lithium ion batteries, it showed good retention of specific capacity (1264.7 mAh g^{-1} even after 150 cycles), decent rate performance and high coulombic efficiency (above 99%). What's more, this procedure to form yolk-shell structure is unique, straightforward and cost-effective, which is significant to enhance the performance of renewable energy materials possessing large volume change.

Acknowledgements

Financial supports from the NSFC (21173037 and 21274017) and the Science Technology Program of Jilin Province (201201064, 20140101087JC) are gratefully acknowledged.

Notes and references

[a]Faculty of Chemistry, Northeast Normal University, Changchun 130024, China. E-mail: sunhz335@nenu.edu.cn; jpzhang@nenu.edu.cn.
[b]State Key Laboratory of Electroanalytical Chemistry, Changchun Institute of Applied Chemistry, Chinese Academy of Sciences, 5625 Renmin Street, 130022 Changchun, P.R. China.

1. C. K. Chan, H. Peng, G. Liu, K. McIlwrath, X. F. Zhang, R. A. Huggins and Y. Cui, *Nat Nano*, 2008, **3**, 31-35.
2. A. M. Chockla, J. T. Harris, V. A. Akhavan, T. D. Bogart, V. C. Holmberg, C. Steinhagen, C. B. Mullins, K. J. Stevenson and B. A. Korgel, *Journal of the American Chemical Society*, 2011, **133**, 20914-20921.
3. J. M. Tarascon and M. Armand, *Nature*, 2001, **414**, 359-367.
4. H. Li and H. Zhou, *Chemical Communications*, 2012, **48**, 1201-1217.
5. G. Liu, S. Xun, N. Vukmirovic, X. Song, P. Olalde-Velasco, H. Zheng, V. S. Battaglia, L. Wang and W. Yang, *Advanced Materials*, 2011, **23**, 4679-4683.
6. M. L. Terranova, S. Orlanducci, E. Tamburri, V. Guglielmotti and M. Rossi, *Journal of Power Sources*, 2014, **246**, 167-177.
7. U. Kasavajjula, C. Wang and A. J. Appleby, *Journal of Power Sources*, 2007, **163**, 1003-1039.
8. H.-C. Tao, L.-Z. Fan and X. Qu, *Electrochimica Acta*, 2012, **71**, 194-200.
9. Y. Yang, J.-G. Ren, X. Wang, Y.-S. Chui, Q.-H. Wu, X. Chen and W. Zhang, *Nanoscale*, 2013, **5**, 8689-8694.
10. H. Wu and Y. Cui, *Nano Today*, 2012, **7**, 414-429.
11. H. Kim and J. Cho, *Nano Letters*, 2008, **8**, 3688-3691.
12. A. Kohandehghan, P. Kalisvaart, K. Cui, M. Kupsta, E. Memarzadeh and D. Mitlin, *Journal of Materials Chemistry A*, 2013, **1**, 12850-12861.
13. J. Wang, Y. Yu, L. Gu, C. Wang, K. Tang and J. Maier, *Nanoscale*, 2013, **5**, 2647-2650.
14. Y. Fan, Q. Zhang, C. Lu, Q. Xiao, X. Wang and B. k. Tay, *Nanoscale*, 2013, **5**, 1503-1506.
15. Y. S. Hu, R. Demir-Cakan, M. M. Titirici, J. O. Müller, R. Schlögl, M. Antonietti and J. Maier, *Angewandte Chemie - International Edition*, 2008, **47**, 1645-1649.
16. Y. Yin, L. Wan and Y. Guo, *Chin. Sci. Bull.*, 2012, **57**, 4104-4110.
17. C. Wang, Y.-S. Chui, R. Ma, T. Wong, J.-G. Ren, Q.-H. Wu, X. Chen and W. Zhang, *Journal of Materials Chemistry A*, 2013, **1**, 10092-10098.
18. J. K. Lee, K. B. Smith, C. M. Hayner and H. H. Kung, *Chemical Communications*, 2010, **46**, 2025-2027.
19. B. Laïk, L. Eude, J.-P. Pereira-Ramos, C. S. Cojocaru, D. Pribat and E. Rouvière, *Electrochimica Acta*, 2008, **53**, 5528-5532.
20. J. Chen, L. Yang, S. Rousidan, S. Fang, Z. Zhang and S.-i. Hirano, *Nanoscale*, 2013, **5**, 10623-10628.
21. S. E. Lee, H.-J. Kim, H. Kim, J. H. Park and D.-G. Choi, *Nanoscale*, 2013, **5**, 8986-8991.
22. B. Wang, X. Li, X. Zhang, B. Luo, Y. Zhang and L. Zhi, *Advanced Materials*, 2013, **25**, 3560-3565.
23. H. Ma, F. Cheng, J. Y. Chen, J. Z. Zhao, C. S. Li, Z. L. Tao and J. Liang, *Advanced Materials*, 2007, **19**, 4067-4070.
24. Y. Yao, M. T. McDowell, I. Ryu, H. Wu, N. Liu, L. Hu, W. D. Nix and Y. Cui, *Nano Letters*, 2011, **11**, 2949-2954.
25. T. Song, J. Xia, J.-H. Lee, D. H. Lee, M.-S. Kwon, J.-M. Choi, J. Wu, S. K. Doo, H. Chang, W. I. Park, D. S. Zang, H. Kim, Y. Huang, K.-C. Hwang, J. A. Rogers and U. Paik, *Nano Letters*, 2010, **10**, 1710-1716.
26. X.-L. Wu, Y.-G. Guo and L.-J. Wan, *Chemistry – An Asian Journal*, 2013, **8**, 1948-1958.
27. I. s. Kim, P. N. Kumta and G. E. Blomgren, *Electrochemical and Solid-State Letters*, 2000, **3**, 493-496.
28. O. Mao, R. L. Turner, I. A. Courtney, B. D. Fredericksen, Buckett, M. I., L. J. Krause and J. R. Dahn, *Electrochemical and Solid-State Letters*, 1999, **2**, 3-5.
29. S. H. Ng, J. Wang, D. Wexler, K. Konstantinov, Z. P. Guo and H. K. Liu, *Angew Chem Int Ed Engl*, 2006, **45**, 6896-6899.
30. P. Zuo, G. Yin and Y. Ma, *Electrochimica Acta*, 2007, **52**, 4878-4883.
31. K. Kamata, Y. Lu and Y. Xia, *Journal of the American Chemical Society*, 2003, **125**, 2384-2385.
32. Y. J. Hong, M. Y. Son, B. K. Park and Y. C. Kang, *Small*, 2013, **9**, 2224-2227.
33. B. Liu, W. Zhang, H. Feng and X. Yang, *Chemical Communications*, 2011, **47**, 11727-11729.
34. J. Liu, J. Xu, R. Che, H. Chen, M. Liu and Z. Liu, *Chemistry – A European Journal*, 2013, **19**, 6746-6752.
35. H. Wan, H. Qin, Z. Xiong, W. Zhang and H. Zou, *Nanoscale*, 2013, **5**, 10936-10944.
36. N. Liu, H. Wu, M. T. McDowell, Y. Yao, C. Wang and Y. Cui, *Nano Letters*, 2012, **12**, 3315-3321.
37. Y. Ru, D. G. Evans, H. Zhu and W. Yang, *RSC Advances*, 2014, **4**, 71-75.
38. X. Li, P. Meduri, X. Chen, W. Qi, M. H. Engelhard, W. Xu, F. Ding, J. Xiao, W. Wang, C. Wang, J.-G. Zhang and J. Liu, *Journal of Materials Chemistry*, 2012, **22**, 11014-11017.
39. S. Chen, M. L. Gordin, R. Yi, G. Howlett, H. Sohn and D. Wang, *Physical Chemistry Chemical Physics*, 2012, **14**, 12741-12745.
40. H. Tao, L.-Z. Fan, W.-L. Song, M. Wu, X. He and X. Qu, *Nanoscale*, 2014, **6**, 3138-3142.
41. X.-y. Zhou, J.-j. Tang, J. Yang, J. Xie and L.-l. Ma, *Electrochimica Acta*, 2013, **87**, 663-668.
42. T. Yao, T. Cui, X. Fang, J. Yu, F. Cui and J. Wu, *Chemical Engineering Journal*, 2013, **225**, 230-236.
43. X. Li and L. Zhi, *Nanoscale*, 2013, **5**, 8864-8873.
44. J. Liu, S. Z. Qiao, J. S. Chen, X. W. Lou, X. Xing and G. Q. Lu, *Chemical Communications*, 2011, **47**, 12578-12591.
45. Z. Bao, M. R. Weatherspoon, S. Shian, Y. Cai, P. D. Graham, S. M. Allan, G. Ahmad, M. B. Dickerson, B. C. Church, Z. Kang, H. W. Abernathy Iii, C. J. Summers, M. Liu and K. H. Sandhage, *Nature*, 2007, **446**, 172-175.
46. J. L. Gomez-Camer, J. Morales and L. Sanchez, *Journal of Materials Chemistry*, 2011, **21**, 811-818.
47. P. F. Fulvio, R. T. Mayes, X. Wang, S. M. Mahurin, J. C. Bauer, V. Presser, J. McDonough, Y. Gogotsi and S. Dai, *Advanced Functional Materials*, 2011, **21**, 2208-2215.
48. M. Kruk and M. Jaroniec, *Chemistry of Materials*, 2001, **13**, 3169-3183.
49. X. H. Liu, L. Zhong, S. Huang, S. X. Mao, T. Zhu and J. Y. Huang, *ACS Nano*, 2012, **6**, 1522-1531.
50. W. Wang, B. Jiang, L. Hu, Z. Lin, J. Hou and S. Jiao, *Journal of Power Sources*, 2014, **250**, 181-187.

51. E. Luais, J. Sakai, S. Desplobain, G. Gautier, F. Tran-Van and F. Ghamouss, *Journal of Power Sources*, 2013, **242**, 166-170.